Light Scattering from Solid-State Quantum Emitters: Beyond the Atomic Picture

Alistair J. Brash,[1,*] Jake Iles-Smith,[1,2,†] Catherine L. Phillips,[1] Dara P. S. McCutcheon,[3] John O'Hara,[1] Edmund Clarke,[4] Benjamin Royall,[1] Luke R. Wilson,[1] Jesper Mørk,[5] Maurice S. Skolnick,[1] A. Mark Fox,[1] and Ahsan Nazir[2]

[1]*Department of Physics and Astronomy, University of Sheffield, Sheffield S3 7RH, United Kingdom*
[2]*Department of Physics and Astronomy, The University of Manchester, Oxford Road, Manchester M13 9PL, United Kingdom*
[3]*Quantum Engineering Technology Labs, H. H. Wills Physics Laboratory and Department of Electrical and Electronic Engineering, University of Bristol, Bristol BS8 1FD, United Kingdom*
[4]*EPSRC National Epitaxy Facility, Department of Electronic and Electrical Engineering, University of Sheffield, Sheffield S1 4DE, United Kingdom*
[5]*Department of Photonics Engineering, DTU Fotonik, Technical University of Denmark, Building 343, 2800 Kongens Lyngby, Denmark*

(Received 11 April 2019; published 16 October 2019)

Coherent scattering of light by a single quantum emitter is a fundamental process at the heart of many proposed quantum technologies. Unlike atomic systems, solid-state emitters couple to their host lattice by phonons. Using a quantum dot in an optical nanocavity, we resolve these interactions in both time and frequency domains, going beyond the atomic picture to develop a comprehensive model of light scattering from solid-state emitters. We find that even in the presence of a low-Q cavity with high Purcell enhancement, phonon coupling leads to a sideband that is completely insensitive to excitation conditions and to a nonmonotonic relationship between laser detuning and coherent fraction, both of which are major deviations from atomlike behavior.

DOI: 10.1103/PhysRevLett.123.167403

The scattering of light by quantum emitters is the foundation of quantum optics. First observed in atoms [1,2] and studied extensively in self-assembled quantum dots (QDs) [3–6], coherent scattering attracts interest as the scattered light retains the coherence of the laser rather than the emitter. As such, the photon coherence may exceed the conventional radiative limit while still exhibiting antibunching on the timescale of the emitter lifetime [3–6]. These properties underpin key quantum technologies such as generating tuneable single photons [7–9], realizing single photon nonlinearities [10–14], and constructing entangled states between photons [15,16] or spins [17,18].

Coherent scattering occurs in the weak excitation regime where photon absorption and emission become a single coherent event. For a two-level "atomic picture" with only radiative decay and pure dephasing, the coherent fraction ($\mathcal{F}_{\mathrm{CS}}$) of the total emission is [19]

$$\mathcal{F}_{\mathrm{CS}} = \frac{T_2}{2T_1}\frac{1}{1+\mathcal{S}}, \tag{1}$$

where $\mathcal{S} = (\Omega^2 T_1 T_2)/(1+\Delta_{\mathrm{LX}}^2 T_2^2)$ is a generalized saturation parameter, Ω is the Rabi frequency, $\Delta_{\mathrm{LX}} = \omega_L - \omega_X$ is the laser (ω_L) and emitter (ω_X) detuning, and T_1 and T_2 are the emitter lifetime and coherence time, respectively. This expression predicts that the fraction of coherently scattered light reaches unity when driving well below saturation ($\mathcal{S} \ll 1$) with transform-limited emitter coherence ($T_2 = 2T_1$).

Solid-state emitters (SSEs), particularly self-assembled QDs, are attractive owing to their high brightness and ease of integration with nanophotonic structures. Unlike atoms, SSEs can experience significant dephasing from fluctuating charges [20,21] and coupling to vibrational modes of the host material [22,23]. Despite this, InGaAs QD single photon sources have demonstrated essentially transform-limited photons emitted into the zero phonon line (ZPL) [24–26] achieved through sample optimization, exploiting photonic structures, and by using resonant π-pulse excitation at cryogenic temperatures. These results show that ZPL broadening can be effectively suppressed, but coupling to vibrational modes also leads to a broad phonon sideband (PSB) in the emission spectrum [23,27–32]. This is attributed to a rapid change in lattice configuration of the host material during exciton recombination and photon emission, leading to the simultaneous emission or absorption of longitudinal acoustic (LA) phonons. Therefore, to obtain perfectly indistinguishable photons, the PSB must be filtered out, naturally limiting the device efficiency, even when using an optical cavity to Purcell enhance emission into the ZPL [31,33].

These studies highlight the importance of phonon coupling in the incoherent resonance fluorescence regime, where there is a definite change of charge configuration in the QD. It is perhaps natural to presume that phonon coupling is eliminated in the coherent scattering regime, since there is vanishing exciton population and therefore no change in charge configuration. This would imply that, in accordance with prior work [3–5], one may adopt the atomlike picture of Eq. (1), where the coherent fraction tends towards unity for excitation far below saturation and transform-limited coherence. However, recent theoretical work predicts the presence of PSBs even at vanishingly weak resonant driving [30].

Here, we experimentally verify that PSBs persist in the coherent scattering regime and demonstrate additionally that phonon processes also cause large deviations from atomlike physics when driving off resonance. By extending the theory presented in Ref. [30] to include an optical cavity, we fully model our solid-state nanocavity system, providing an intuitive picture that attributes the PSB to phonon dressing of the optical dipole moment. This leads to a finite probability that the vibrational environment changes state during a scattering event, implying that all optical spectral features will have an associated PSB. While a QD is studied here, the physics and methods apply to a diverse range of SSEs, including diamond vacancy centers [34,35], carbon nanotubes [36], and defects in hexagonal boron nitride [37,38].

We study a neutral exciton ($|X\rangle$) in a self-assembled InGaAs QD that is weakly coupled ($\hbar g = 135\ \mu$eV) to a photonic crystal cavity (linewidth $\hbar\kappa = 2.51$ meV). A previous study of this device [26] established $T_2 = 2T_1$ under weak resonant excitation and a Purcell factor $F_P = 43$ when the QD transition was centred on the cavity mode. Here, the transition is detuned 0.4 meV to higher energy, reducing F_P to ~37 corresponding to $T_1 = 25$ ps [26]. As well as Purcell enhancement, the cavity also acts as a weak spectral filter; this combination reduces the PSB component of the emission [31,33]. Figure 1(a) illustrates the experiment: The sample is held at $T = 4.2$ K and excited by a tuneable laser that is rejected by cross-polarized detection (typical signal to background $>100:1$). The coherence of the scattered light is studied either in the time domain by measuring fringe contrast $v(\tau)$ with a Mach-Zehnder interferometer or in the frequency domain using a spectrometer or a Fabry-Perot interferometer (FPI) (details in the Supplemental Material [39]).

We begin with a high resolution time-domain measurement, exciting resonantly below saturation ($\mathcal{S} = 0.25$) where coherent scattering is expected to dominate. The measured fringe contrast $v(\tau)$ is proportional to the envelope of the first-order correlation function $g^{(1)}(\tau)$ [39]. The result in Fig. 1(b) departs significantly from the monoexponential radiative decay predicted by atomic theory (dashed line); a rapid decay of coherence occurs in the first few picoseconds, comparable to phonon dynamics observed in pulsed four-wave mixing measurements of InGaAs QDs in the incoherent regime [40–42], suggesting that the rapid loss of coherence we observe originates from electron-phonon interactions.

To describe this behavior, we account for the microscopic nature of the QD-phonon coupling [43] by applying the polaron transformation to the full system-environment Hamiltonian. This dresses the excitonic states of the system with phonon modes, allowing derivation of a QD master equation (ME) that is nonperturbative in the electron-phonon

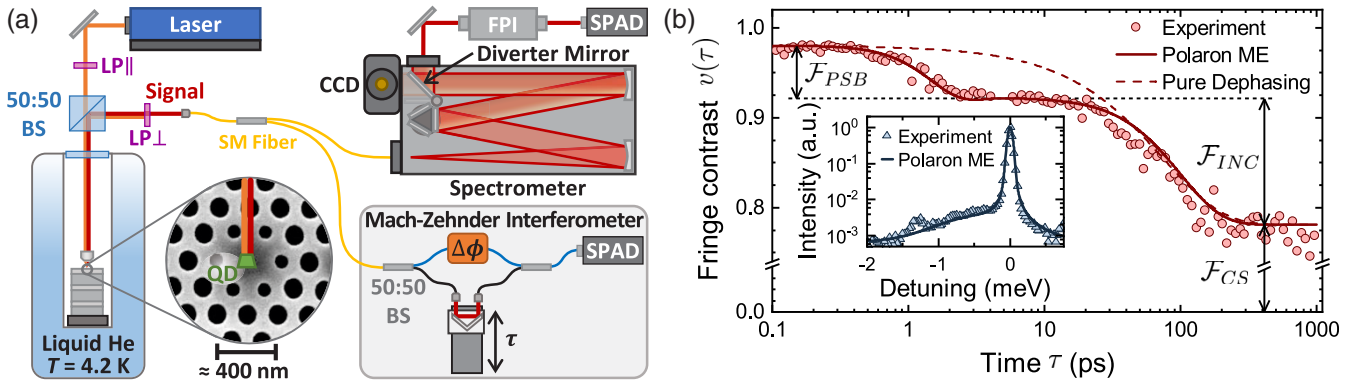

FIG. 1. (a) Schematic of the experiment: BS, beam splitter; CCD, charge-coupled device (camera); FPI, Fabry-Perot interferometer; LP, linear polarizer; SM, single mode fiber; SPAD, single photon avalanche diode; $\Delta\phi$, phase shift; τ path length difference. (b) Measurement of the first-order correlation function $[g^{(1)}(\tau)]$ at $\mathcal{S} = 0.25$ with $\Delta_{LX} = 0$. The emission contains a phonon sideband ($\mathcal{F}_{PSB}$), incoherent resonance fluorescence ($\mathcal{F}_{inc}$), and coherently scattered ($\mathcal{F}_{CS}$) fractions. Experimental measurements of fringe contrast (red circles) agree well with a calculation using the polaron master equation (solid red line) where the phonon coupling strength α and cutoff frequency ν_c are the only free parameters. A pure dephasing model (dashed red line) decays monoexponentially and cannot capture phonon dynamics. Inset: An experimental spectrum (blue triangles) measured simultaneously is also well reproduced by the polaron model (blue line) with the same parameters. The calculated spectrum is convolved with the spectrometer instrument response in order to reproduce the observed ZPL width.

coupling strength [30,39,44–46]. In the polaron frame, the first-order correlation function is $g^{(1)}_{\mathrm{pol}}(\tau) = \mathcal{G}(\tau) g^{(1)}_{\mathrm{opt}}(\tau)$ [30], where $g^{(1)}_{\mathrm{opt}}(\tau)$ is the purely optical contribution found using the polaron frame ME, while $\mathcal{G}(\tau) = B^2 \exp[\varphi(\tau)]$ is the phonon environment correlation function accounting for non-Markovian phonon relaxation. The response of the phonon environment to the exciton dynamics is contained within the phonon propagator $\varphi(\tau) = \alpha \int_0^\infty \nu e^{-\nu^2/\nu_c^2} [\cos(\nu\tau)\coth(\nu/2k_BT) - i\sin(\nu\tau)] d\nu$ and the Franck-Condon factor $B = \exp[-\varphi(0)/2]$. We refer the reader to the Supplemental Material [39] for a detailed discussion of these terms. The QD-phonon coupling is thus specified by the thermal energy k_BT, the deformation potential coupling strength α, and the cutoff frequency ν_c [27,43,47]. The cavity leads both to Purcell-enhanced ZPL decay (included within the ME) and spectral filtering of the emission [31]. To go beyond the theory presented in Ref. [30], we must formally incorporate cavity filtering into the steady-state correlation function. This is done by solving the Heisenberg equations of motion for the cavity field operators, taking careful account of the time ordering of the appropriate operators [39]. This leads to the detected correlation function

$$g^{(1)}_D(\tau) = \int_{-\infty}^{\infty} \tilde{h}(t-\tau) g^{(1)}_{\mathrm{pol}}(t) dt, \tag{2}$$

where $\tilde{h}(t) = \exp(-i\Delta_{\mathrm{XC}} t - \kappa|t|/2)$ is the cavity filter function, and Δ_{XC} is the exciton-cavity detuning [39].

By fitting the phonon part of Eq. (2) to the first few picoseconds of the measurement, we extract $\alpha = 0.045$ ps^2 and $\nu_c = 1.3\,\mathrm{ps}^{-1}$, comparable to previous InGaAs QD values [48]. Fixing all other parameters to independently measured values, we accurately reproduce the full experimental dynamics [solid line in Fig. 1(b)]. After phonon relaxation, radiative decay associated with incoherent resonance fluorescence occurs between $\tau = 20$ and 200 ps. Finally, at $\tau \gg 200$ ps, $v(\tau)$ plateaus, corresponding to the coherent fraction of the emission which inherits the laser coherence. From the $v(\tau)$ amplitudes, we extract $\mathcal{F}_{\mathrm{PSB}} = 0.06$, $\mathcal{F}_{\mathrm{inc}} = 0.14$, and $\mathcal{F}_{\mathrm{CS}} = 0.80$ for the PSB, incoherent, and coherent fractions of the total emission ($\mathcal{F}$), respectively. A finite $\mathcal{F}_{\mathrm{PSB}}$ at weak driving indicates that Eq. (1) does not fully describe the measurements.

To verify these parameters, we move to the frequency domain, where the intensity as a function of emission frequency (ω) is calculated by Fourier transforming $g^{(1)}_D(\tau)$ and may be written as $S(\omega) = H(\omega)[S_{\mathrm{opt}}(\omega) + S_{\mathrm{SB}}(\omega)]$, where $H(\omega) = (\kappa/2)/[(\omega - \Delta_{\mathrm{XC}})^2 + (\kappa/2)^2]$ is the frequency-domain cavity filter function [31,49,50]. The spectrum contains both a purely optical part,

$$S_{\mathrm{opt}}(\omega) = B^2 \int_{-\infty}^{\infty} g_{\mathrm{opt}}(\tau) e^{i\omega\tau} d\tau, \tag{3}$$

with coherent and incoherent contributions, and a second incoherent component,

$$S_{\mathrm{SB}}(\omega) = \int_{-\infty}^{\infty} [\mathcal{G}(\tau) - B^2] g_{\mathrm{opt}}(\tau) e^{i\omega\tau} d\tau, \tag{4}$$

which gives rise to the PSB [30,31]. The ZPL contribution is thus reduced by the square of the constant Franck-Condon factor B^2, with the missing fraction emitted through the PSB.

Figure 1(b) (inset) illustrates that the parameters extracted from the time-domain dynamics lead to excellent agreement between the experimental (blue triangles) and theoretical (solid line) spectra, with a broad PSB observed in accordance with the short timescale of the phonon processes. These combined time- and frequency-domain measurements provide critical insight into the nature of electron-phonon interactions in driven QDs: Even well below saturation, where the excited-state population is small and coherent scattering dominates, a PSB is present, comprising ~6% of the emission.

We now measure the resonance fluorescence spectrum as a function of the saturation by varying Ω. Figure 2(a) shows a spectrum taken well above saturation ($\mathcal{S} = 10$) exhibiting a ZPL (yellow fit) and a PSB [$S_{\mathrm{SB}}(\omega)$, red fit]. High resolution spectroscopy of the ZPL with the FPI results in the inset of Fig. 2(a), which exhibits a broad linewidth ($2/T_2 \approx 25$ μeV, transform limited) contribution from incoherent resonance fluorescence (blue fit) and a narrow feature from coherent scattering (green fit). As in the time domain, the total spectrum thus comprises three components whose fraction of the total emission can be evaluated from their areas (details in Ref. [39]).

Figure 2(b) shows the evolution of the components of the resonant ($\Delta_{\mathrm{LX}} = 0$) scattering spectrum as a function of $\mathcal{S}$. The polaron model agrees well with the experiment and produces a curve for $\mathcal{F}_{\mathrm{CS}}$ (green dashed line) that is proportional to $(1+\mathcal{S})^{-1}$ like Eq. (1). However, as previously predicted [30], $\mathcal{F}_{\mathrm{CS}}$ does not reach unity for vanishing $\mathcal{S}$, a surprising result that may be explained by observing that the PSB fraction $\mathcal{F}_{\mathrm{PSB}}$ (red diamonds) is independent of Ω. This contrasts with excitation-induced dephasing (EID), another process captured in our model that arises from LA phonon mediated transitions between the dressed states of the optically excited emitter [48,51]. For EID, the rate is proportional to $(\Omega^2 + \Delta^2_{\mathrm{LX}})$ and thus is negligible for resonant driving below saturation.

The results of Fig. 2(b) can be understood by considering the possible scattering channels illustrated in Figs. 2(c) and 2(d). The optical transition $|0\rangle \rightarrow |X\rangle$ (solid black levels) is dressed with vibronic bands corresponding to emission or absorption of a LA phonon (gray shading). In the simplest case [Fig. 2(c)], a laser photon coherently (Rayleigh) scatters directly from the exciton transition. However, the phonon dressing of the optical transition results in

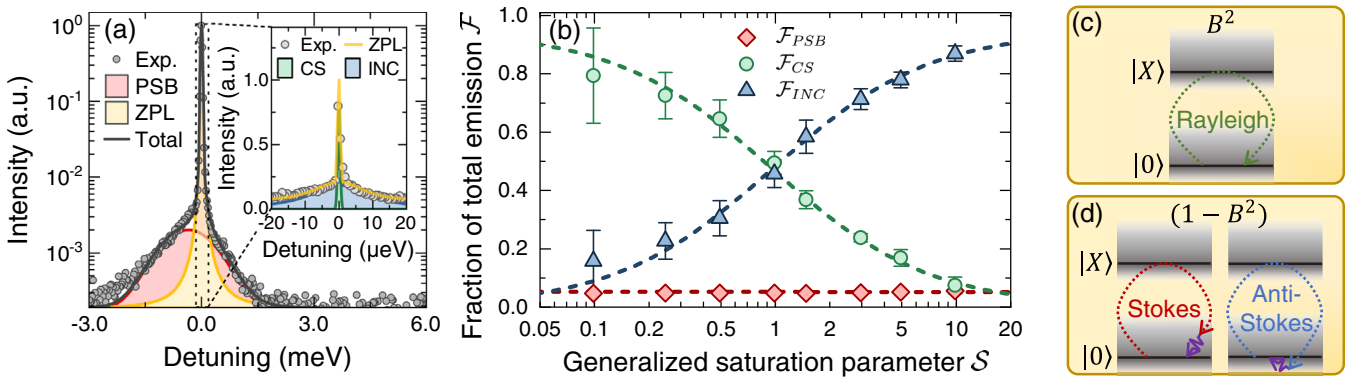

FIG. 2. Components of the resonant scattering spectrum. (a) Semilog spectrum at low resolution ($\mathcal{S} = 10$, $\Delta_{LX} = 0$): gray circles, experiment; yellow, fit to ZPL; red, fit to PSB; black line, total fit. Inset: High resolution spectrum. Gray circles, experiment; green, fit to coherent scattering; blue, fit to incoherent resonance fluorescence; yellow, total fitted profile. (b) Evolution with increasing Ω: red diamonds, PSB; green circles, coherent scattering; blue triangles, incoherent resonance fluorescence; dashed lines, polaron model. (c) Coherent scattering occurs when laser photons scatter directly from the bare transition (solid black lines) with probability given by the square of the Franck-Condon factor (B^2). (d) Inelastic scattering occurs when the system scatters [with probability $(1 - B^2)$] into a different vibrational state within the ground-state manifold (gray shading). A LA phonon (purple) is emitted or absorbed for the Stokes and anti-Stokes cases, respectively.

nonzero overlaps between vibronic states in the ground- and excited-state manifolds, such that a scattering event can end in a different vibrational state within the ground-state manifold [Fig. 2(d)]. This corresponds to inelastic Stokes (anti-Stokes) scattering of a lower- (higher-) energy photon accompanied by the emission (absorption) of a LA phonon, leading to the emergence of a PSB. At low temperatures, phonon absorption is suppressed, resulting in the characteristically asymmetric PSB. From Eqs. (3) and (4), the branching ratio between phonon-mediated inelastic and elastic scattering is determined solely by the constant B^2. Outside the Mollow triplet regime, the coherent ($\mathcal{S} \ll 1$) and incoherent ($\mathcal{S} \gtrsim 1$) resonant scattering spectra of a SSE thus differ only in the width of the ZPL. As such, while coherent scattering is often cited as a route to highly coherent single photons, it cannot negate the PSB.

To gain further insight, we consider the effect of detuning the laser from the emitter. Figure 3(a) shows spectra taken at constant Ω with laser detuning $\hbar\Delta_{LX} = \pm 0.27$ meV. The coherent peaks at $\hbar\Delta_{LX}$ are separated from the ZPL and dominate the spectrum. For positive detuning (blue), it is noticeable that the high-energy edge of the sideband is shifted by $\sim\hbar\Delta_{LX}$. Considering Eq. (4), we see the time-domain product implies a convolution in frequency between the purely optical spectrum and the frequency-space phonon correlation function. As such, all optical features in S_{opt} have an associated PSB; the coherent peak (and associated PSB) shifts with Δ_{LX}, but the total

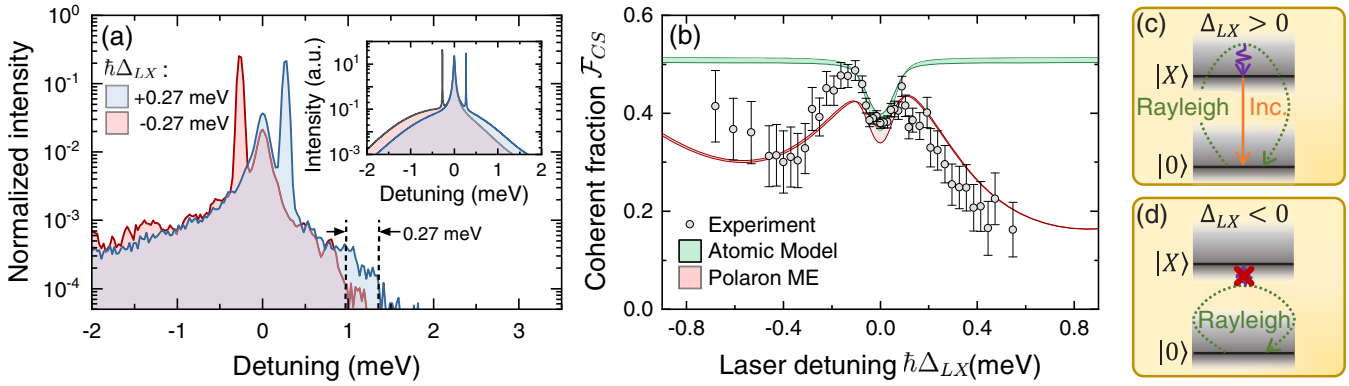

FIG. 3. Phonon influences in detuned ($\Delta_{LX} \neq 0$) coherent scattering. (a) Semilog spectra (normalized by integrated intensity) for $\Delta_{LX} = \pm 0.27$ meV (blue/red) at constant $\hbar\Omega = 5.7$ μeV. Inset: Theoretical spectrum. (b) $\mathcal{F}_{CS}$ vs Δ_{LX} at constant $\hbar\Omega = 25.6$ μeV: gray circles, experimental $\mathcal{F}_{CS}$ extracted as in Fig. 1(b); red lines, polaron master equation; green lines, atomic model, both models include additional pure dephasing and spectral wandering [39] and have upper and lower bounds from uncertainty in Ω. (c) For $\Delta_{LX} > 0$, emission of a LA phonon can populate $|X\rangle$, allowing incoherent relaxation. (d) For $\Delta_{LX} < 0$, populating $|X\rangle$ requires LA phonon absorption which is weak at $T = 4.2$ K.

PSB fraction is still a constant B^2. Theoretically [Fig. 3(a) inset], we also expect the low-energy edge of the PSB to shift for negative detuning (red spectrum); experimentally, this is obscured by weak incoherent backgrounds owing to low count rates at large Δ_{LX}.

Further deviations from atomic behavior can be seen when driving off resonance. Compared to the experiment, both the atomic and polaron theories significantly overestimate the coherent fraction off resonance. We tentatively suggest that this is due to the reduced scattering cross section of the QD when driving off resonance, allowing detuned laser light to instead be absorbed by the doped bulk material [52], leading to charge noise. To capture the associated detuning-dependent dephasing $\gamma(\Delta_{LX})$ in both the atomic and polaron models, we assume a Lorentzian profile with width fixed to the QD natural linewidth ($1/T_1 = 25\ \mu$eV) [39], mimicking the absorption profile of the QD. We find the amplitude of $\gamma(\Delta_{LX})$ to be $\gamma_{max} = 21\ \mu$eV by fitting the data, with $\gamma(0) = 0$ reflecting the transform-limited coherence observed for resonant driving in Fig. 2. Spectral wandering is then accounted for by convolving with a Gaussian noise function [39].

In Fig. 3(b), bounds (from uncertainty in Ω) of the atomic (green) and polaron (red) models are plotted. Experimentally (gray circles), $\mathcal{F}_{CS}$ is evaluated as in Fig. 1(b). In contrast to the atomic theory, where Eq. (1) predicts $\mathcal{F}_{CS}$ only ever increases with $|\Delta_{LX}|$, the measured data only increase close to resonant driving where EID [48,51] is small. For 0.1 meV $< |\Delta_{LX}| <$ 0.4 meV, EID becomes significant and the coherent fraction decreases with a noticeable asymmetry, as predicted by the polaron model. This asymmetry originates from the phonon dressing of the optical transition; when $\Delta_{LX} > 0$ [Fig. 3(c)], $|X\rangle$ can be populated through the emission of a LA phonon [53–55] (purple arrow), increasing incoherent scattering (orange arrow). For $\Delta_{LX} < 0$ [Fig. 3(d)], populating $|X\rangle$ is inhibited at $T = 4.2$ K as it requires phonon absorption [56,57]; for $\Delta_{LX} < -0.5$ meV, this becomes sufficiently weak that $\mathcal{F}_{CS}$ begins to increase again towards the limiting atomic case. This deviation from the atomic model has implications for schemes involving detuned coherent scattering, such as generating single [8,9] or entangled [15,16] photons.

We have shown that a fixed fraction of light scattered from a solid-state emitter is always lost through a phonon sideband, irrespective of excitation conditions such as Rabi frequency or detuning. Furthermore, the detuning dependence of the coherent fraction is strongly modified by the presence of phonon coupling, contradicting the atomic prediction that the coherent fraction will increase monotonically with detuning. These results can be understood by considering phonon dressing of the optical transition of the QD and illustrate the importance of employing an appropriate model of phonon coupling rather than assuming atomlike physics when driving weakly or off resonance. For example, treating phonons in a pure-dephasing approximation [e.g., Eq. (1)] suggests they may be suppressed simply by increasing the Purcell factor. This is directly contradicted by the clear separation of phonon and radiative timescales in Fig. 1(b), with the phonon sideband persisting despite a large Purcell enhancement. Although a high-Q cavity would increase the fraction of light coherently scattered from the emitter, this cannot be done arbitrarily due to the emergence of additional phonon-induced dephasing [31]. The methods developed here can be used to optimize quantum information protocols such as spin-photon entanglement schemes for realistic solid-state emitters.

This work was funded by the Engineering and Physical Sciences Research Council (EPSRC) (UK) Grant No. EP/N031776/1. A. N. is supported by the EPSRC (UK) Grant No. EP/N008154/1, and J. I. S. acknowledges support from the Royal Commission for the Exhibition of 1851.

Note added.—Recently, we became aware of related results [58]. We thank B. D. Gerardot for bringing these to our attention.

*a.brash@sheffield.ac.uk
†Jakeilessmith@gmail.com

[1] H. M. Gibbs and T. N. C. Venkatesan, Direct observation of fluorescence narrower than the natural linewidth, Opt. Commun. **17**, 87 (1976).
[2] J. Volz, M. Weber, D. Schlenk, W. Rosenfeld, C. Kurtsiefer, and H. Weinfurter, An atom and a photon, Laser Phys. **17**, 1007 (2007).
[3] H. S. Nguyen, G. Sallen, C. Voisin, P. Roussignol, C. Diederichs, and G. Cassabois, Ultra-coherent single photon source, Appl. Phys. Lett. **99**, 261904 (2011).
[4] C. Matthiesen, A. N. Vamivakas, and M. Atatüre, Subnatural Linewidth Single Photons from a Quantum Dot, Phys. Rev. Lett. **108**, 093602 (2012).
[5] R. Proux, M. Maragkou, E. Baudin, C. Voisin, P. Roussignol, and C. Diederichs, Measuring the Photon Coalescence Time Window in the Continuous-Wave Regime for Resonantly Driven Semiconductor Quantum Dots, Phys. Rev. Lett. **114**, 067401 (2015).
[6] A. J. Bennett, J. P. Lee, D. J. P. Ellis, T. Meany, E. Murray, F. F. Floether, J. P. Griffths, I. Farrer, D. A. Ritchie, and A. J. Shields, Cavity-enhanced coherent light scattering from a quantum dot, Sci. Adv. **2**, e1501256 (2016).
[7] C. Matthiesen, M. Geller, C. H. H. Schulte, C. Le Gall, J. Hansom, Z. Li, M. Hugues, E. Clarke, and M. Atature, Phase-locked indistinguishable photons with synthesized waveforms from a solid-state source, Nat. Commun. **4**, 1600 (2013).
[8] Y. He, Y.-M. He, Y.-J. Wei, X. Jiang, M.-C. Chen, F.-L. Xiong, Y. Zhao, C. Schneider, M. Kamp, S. Höfling, C.-Y. Lu, and J.-W. Pan, Indistinguishable Tunable Single Photons Emitted by Spin-Flip Raman Transitions in InGaAs Quantum Dots, Phys. Rev. Lett. **111**, 237403 (2013).

[9] T. M. Sweeney, S. G. Carter, A. S. Bracker, M. Kim, C. S. Kim, L. Yang, P. M. Vora, P. G. Brereton, E. R. Cleveland, and D. Gammon, Cavity-stimulated raman emission from a single quantum dot spin, Nat. Photonics **8**, 442 (2014).

[10] A. Javadi, I. Sllner, M. Arcari, S. L. Hansen, L. Midolo, S. Mahmoodian, G. Kiransk, T. Pregnolato, E. H. Lee, J. D. Song, S. Stobbe, and P. Lodahl, Single-photon non-linear optics with a quantum dot in a waveguide, Nat. Commun. **6**, 8655 (2015).

[11] A. Sipahigil, R. E. Evans, D. D. Sukachev, M. J. Burek, J. Borregaard, M. K. Bhaskar, C. T. Nguyen, J. L. Pacheco, H. A. Atikian, C. Meuwly, R. M. Camacho, F. Jelezko, E. Bielejec, H. Park, M. Lončar, and M. D. Lukin, An integrated diamond nanophotonics platform for quantum optical networks, Science **354**, 847 (2016).

[12] A. J. Bennett, J. P. Lee, D. J. P. Ellis, I. Farrer, D. A. Ritchie, and A. J. Shields, A semiconductor photon-sorter, Nat. Nanotechnol. **11**, 857 (2016).

[13] L. De Santis, C. Antón, B. Reznychenko, N. Somaschi, G. Coppola, J. Senellart, C. Gómez, A. Lemaître, I. Sagnes, A. G. White, L. Lanco, A. Auffèves, and P. Senellart, A solid-state single-photon filter, Nat. Nanotechnol. **12**, 663 (2017).

[14] D. Hallett, A. P. Foster, D. L. Hurst, B. Royall, P. Kok, E. Clarke, I. E. Itskevich, A. M. Fox, M. S. Skolnick, and L. R. Wilson, Electrical control of nonlinear quantum optics in a nano-photonic waveguide, Optica **5**, 644 (2018).

[15] E. V. Denning, J. Iles-Smith, D. P. S. McCutcheon, and J. Mork, Protocol for generating multiphoton entangled states from quantum dots in the presence of nuclear spin fluctuations, Phys. Rev. A **96**, 062329 (2017).

[16] D. Scerri, R. N. E. Malein, B. D. Gerardot, and E. M. Gauger, Frequency-encoded linear cluster states with coherent Raman photons, Phys. Rev. A **98**, 022318 (2018).

[17] A. Delteil, Z. Sun, W.-b. Gao, E. Togan, S. Faelt, and A. Imamolu, Generation of heralded entanglement between distant hole spins, Nat. Phys. **12**, 218 (2016).

[18] R. Stockill, M. J. Stanley, L. Huthmacher, E. Clarke, M. Hugues, A. J. Miller, C. Matthiesen, C. Le Gall, and M. Atatüre, Phase-Tuned Entangled State Generation between Distant Spin Qubits, Phys. Rev. Lett. **119**, 010503 (2017).

[19] Equation (1) generalizes expressions from C. Cohen-Tannoudji, J. Dupont-Roc, and G. Grynberg, *Atom-Photon Interactions: Basic Processes and Applications* (Wiley-VCH, New York, 1998), pp. 369, 383 to include pure dephasing.

[20] J. Houel, A. V. Kuhlmann, L. Greuter, F. Xue, M. Poggio, B. D. Gerardot, P. A. Dalgarno, A. Badolato, P. M. Petroff, A. Ludwig, D. Reuter, A. D. Wieck, and R. J. Warburton, Probing Single-Charge Fluctuations at a GaAs/AlAs Interface Using Laser Spectroscopy on a Nearby InGaAs Quantum Dot, Phys. Rev. Lett. **108**, 107401 (2012).

[21] A. V. Kuhlmann, J. Houel, A. Ludwig, L. Greuter, D. Reuter, A. D. Wieck, M. Poggio, and R. J. Warburton, Charge noise and spin noise in a semiconductor quantum device, Nat. Phys. **9**, 570 (2013).

[22] E. A. Muljarov and R. Zimmermann, Dephasing in Quantum Dots: Quadratic Coupling to Acoustic Phonons, Phys. Rev. Lett. **93**, 237401 (2004).

[23] A. Reigue, J. Iles-Smith, F. Lux, L. Monniello, M. Bernard, F. Margaillan, A. Lemaitre, A. Martinez, D. P. S. McCutcheon, J. Mørk, R. Hostein, and V. Voliotis, Probing Electron-Phonon Interaction through Two-Photon Interference in Resonantly Driven Semiconductor Quantum Dots, Phys. Rev. Lett. **118**, 233602 (2017).

[24] N. Somaschi, V. Giesz, L. De Santis, J. C. Loredo, M. P. Almeida, G. Hornecker, S. L. Portalupi, T. Grange, C. Antn, J. Demory, C. Gmez, I. Sagnes, N. D. Lanzillotti-Kimura, A. Lematre, A. Auffeves, A. G. White, L. Lanco, and P. Senellart, Near-optimal single-photon sources in the solid state, Nat. Photonics **10**, 340 (2016).

[25] H. Wang, Z.-C. Duan, Y.-H. Li, S. Chen, J.-P. Li, Y.-M. He, M.-C. Chen, Y. He, X. Ding, C.-Z. Peng, C. Schneider, M. Kamp, S. Höfling, C.-Y. Lu, and J.-W. Pan, Near-Transform-Limited Single Photons from an Efficient Solid-State Quantum Emitter, Phys. Rev. Lett. **116**, 213601 (2016).

[26] F. Liu, A. J. Brash, J. OHara, L. M. P. P. Martins, C. L. Phillips, R. J. Coles, B. Royall, E. Clarke, C. Bentham, N. Prtljaga, I. E. Itskevich, L. R. Wilson, M. S. Skolnick, and A. M. Fox, High Purcell factor generation of indistinguishable on-chip single photons, Nat. Nanotechnol. **13**, 835 (2018).

[27] B. Krummheuer, V. M. Axt, and T. Kuhn, Theory of pure dephasing and the resulting absorption line shape in semiconductor quantum dots, Phys. Rev. B **65**, 195313 (2002).

[28] P. Kaer and J. Mørk, Decoherence in semiconductor cavity QED systems due to phonon couplings, Phys. Rev. B **90**, 035312 (2014).

[29] D. P. S. McCutcheon, Optical signatures of non-Markovian behavior in open quantum systems, Phys. Rev. A **93**, 022119 (2016).

[30] J. Iles-Smith, D. P. S. McCutcheon, J. Mørk, and A. Nazir, Limits to coherent scattering and photon coalescence from solid-state quantum emitters, Phys. Rev. B **95**, 201305(R) (2017).

[31] J. Iles-Smith, D. P. S. McCutcheon, A. Nazir, and J. Mørk, Phonon scattering inhibits simultaneous near-unity efficiency and indistinguishability in semiconductor single-photon sources, Nat. Photonics **11**, 521 (2017).

[32] L. Besombes, K. Kheng, L. Marsal, and H. Mariette, Acoustic phonon broadening mechanism in single quantum dot emission, Phys. Rev. B **63**, 155307 (2001).

[33] T. Grange, N. Somaschi, C. Antón, L. De Santis, G. Coppola, V. Giesz, A. Lemaître, I. Sagnes, A. Auffèves, and P. Senellart, Reducing Phonon-Induced Decoherence in Solid-State Single-Photon Sources with Cavity Quantum Electrodynamics, Phys. Rev. Lett. **118**, 253602 (2017).

[34] A. Faraon, P. E. Barclay, C. Santori, K.-M. C. Fu, and R. G. Beausoleil, Resonant enhancement of the zero-phonon emission from a colour centre in a diamond cavity, Nat. Photonics **5**, 301 (2011).

[35] E. Neu, D. Steinmetz, J. Riedrich-Mller, S. Gsell, M. Fischer, M. Schreck, and C. Becher, Single photon emission from silicon-vacancy colour centres in chemical vapour deposition nano-diamonds on iridium, New J. Phys. **13**, 025012 (2011).

[36] A. Jeantet, Y. Chassagneux, C. Raynaud, P. Roussignol, J. S. Lauret, B. Besga, J. Estève, J. Reichel, and C. Voisin, Widely Tunable Single-Photon Source from a Carbon

Nanotube in the Purcell Regime, Phys. Rev. Lett. **116**, 247402 (2016).

[37] N. R. Jungwirth and G. D. Fuchs, Optical Absorption and Emission Mechanisms of Single Defects in Hexagonal Boron Nitride, Phys. Rev. Lett. **119**, 057401 (2017).

[38] D. Wigger, R. Schmidt, O. D. Pozo-Zamudio, J. A. Preuß, P. Tonndorf, R. Schneider, P. Steeger, J. Kern, Y. Khodaei, J. Sperling, S. M. de Vasconcellos, R. Bratschitsch, and T. Kuhn, Phonon-assisted emission and absorption of individual color centers in hexagonal boron nitride, 2D Mater. **6**, 035006 (2019).

[39] See Supplemental Material at http://link.aps.org/supplemental/10.1103/PhysRevLett.123.167403 for a detailed description of the model, experimental methods, and the relationship between them.

[40] A. Vagov, V. M. Axt, T. Kuhn, W. Langbein, P. Borri, and U. Woggon, Nonmonotonous temperature dependence of the initial decoherence in quantum dots, Phys. Rev. B **70**, 201305(R) (2004).

[41] P. Borri, W. Langbein, U. Woggon, V. Stavarache, D. Reuter, and A. D. Wieck, Exciton dephasing via phonon interactions in InAs quantum dots: Dependence on quantum confinement, Phys. Rev. B **71**, 115328 (2005).

[42] T. Jakubczyk, V. Delmonte, S. Fischbach, D. Wigger, D. E. Reiter, Q. Mermillod, P. Schnauber, A. Kaganskiy, J.-H. Schulze, A. Strittmatter, S. Rodt, W. Langbein, T. Kuhn, S. Reitzenstein, and J. Kasprzak, Impact of phonons on dephasing of individual excitons in deterministic quantum dot microlenses, ACS Photonics **3**, 2461 (2016).

[43] A. Nazir and D. P. S. McCutcheon, Modelling exciton–phonon interactions in optically driven quantum dots, J. Phys. Condens. Matter **28**, 103002 (2016).

[44] H.-P. Breuer *et al.*, *The Theory of Open Quantum Systems* (Oxford University Press on Demand, New York, 2002).

[45] D. P. S. McCutcheon and A. Nazir, Quantum dot Rabi rotations beyond the weak exciton–phonon coupling regime, New J. Phys. **12**, 113042 (2010).

[46] C. Roy and S. Hughes, Phonon-Dressed Mollow Triplet in the Regime of Cavity Quantum Electrodynamics: Excitation-Induced Dephasing and Nonperturbative Cavity Feeding Effects, Phys. Rev. Lett. **106**, 247403 (2011).

[47] M. Glässl, M. D. Croitoru, A. Vagov, V. M. Axt, and T. Kuhn, Influence of the pulse shape and the dot size on the decay and reappearance of Rabi rotations in laser driven quantum dots, Phys. Rev. B **84**, 125304 (2011).

[48] A. J. Ramsay, A. V. Gopal, E. M. Gauger, A. Nazir, B. W. Lovett, A. M. Fox, and M. S. Skolnick, Damping of Exciton Rabi Rotations by Acoustic Phonons in Optically Excited InGaAs/GaAs Quantum Dots, Phys. Rev. Lett. **104**, 017402 (2010).

[49] K. Roy-Choudhury and S. Hughes, Quantum theory of the emission spectrum from quantum dots coupled to structured photonic reservoirs and acoustic phonons, Phys. Rev. B **92**, 205406 (2015).

[50] E. V. Denning, J. Iles-Smith, A. D. Osterkryger, N. Gregersen, and J. Mork, Cavity-waveguide interplay in optical resonators and its role in optimal single-photon sources, Phys. Rev. B **98**, 121306(R) (2018).

[51] A. Ulhaq, S. Weiler, C. Roy, S. M. Ulrich, M. Jetter, S. Hughes, and P. Michler, Detuning-dependent Mollow triplet of a coherently-driven single quantum dot, Opt. Express **21**, 4382 (2013).

[52] H. C. Casey, D. D. Sell, and K. W. Wecht, Concentration dependence of the absorption coefficient for *n*- and *p*-type GaAs between 1.3 and 1.6 eV, J. Appl. Phys. **46**, 250 (1975).

[53] M. Glässl, A. M. Barth, and V. M. Axt, Proposed Robust and High-Fidelity Preparation of Excitons and Biexcitons in Semiconductor Quantum Dots Making Active Use of Phonons, Phys. Rev. Lett. **110**, 147401 (2013).

[54] S. Hughes and H. J. Carmichael, Phonon-mediated population inversion in a semiconductor quantum-dot cavity system, New J. Phys. **15**, 053039 (2013).

[55] J. H. Quilter, A. J. Brash, F. Liu, M. Glässl, A. M. Barth, V. M. Axt, A. J. Ramsay, M. S. Skolnick, and A. M. Fox, Phonon-Assisted Population Inversion of a Single InGaAs/GaAs Quantum Dot by Pulsed Laser Excitation, Phys. Rev. Lett. **114**, 137401 (2015).

[56] F. Liu, L. M. P. Martins, A. J. Brash, A. M. Barth, J. H. Quilter, V. M. Axt, M. S. Skolnick, and A. M. Fox, Ultrafast depopulation of a quantum dot by LA-phonon-assisted stimulated emission, Phys. Rev. B **93**, 161407(R) (2016).

[57] A. J. Brash, L. M. P. P. Martins, A. M. Barth, F. Liu, J. H. Quilter, M. Glässl, V. M. Axt, A. J. Ramsay, M. S. Skolnick, and A. M. Fox, Dynamic vibronic coupling in InGaAs quantum dots, J. Opt. Soc. Am. B **33**, C115 (2016).

[58] Z.-X. Koong, D. Scerri, M. Rambach, T. S. Santana, S.-I. Park, J. D. Song, E. M. Gauger, and B. D. Gerardot, preceding Letter, Fundamental Limits to Coherent Photon Generation with Solid-State Atom-Like Transitions, Phys. Rev. Lett. **123**, 167402 (2019).